CDF note 10394

Measurement of $Z/\gamma^* \to e^+e^-$ + jets Production Cross Section

The CDF Collaboration
URL http://www-cdf.fnal.gov

(Dated: January 31, 2011)

Preliminary results on inclusive Z/γ^* boson plus jets production in $\mathrm{p\bar{p}}$ collisions at $\sqrt{\mathrm{s}} = 1.96$ TeV are presented. The measurement is based on 6.2 fb^{-1} of data collected with the CDF detector in run II. Inclusive jet cross sections are measured as a function of p_T^{jet} and jet multiplicity for jets in the region $p_T^{jet} \geqslant 30$ GeV/c and $|y^{jet}| \leqslant 2.1$, in events in which the Z/γ^* boson decays into an electron-positron pair. Results are compared to next-to-leading order perturbative QCD predictions.

I. INTRODUCTION

The measurement of the inclusive production of collimated jets of hadrons in association with a Z/γ^* boson in p$\bar{\text{p}}$ collisions provides a stringent test of perturbative QCD [1]. The Z/γ^* + jets final state is also one of the main backgrounds in searches for new physics like, for example, the Higgs boson in the Z + H channel, and supersymmetry in the $\not{E}_T$ + jets channel. We report on preliminary measurement of $Z/\gamma^* \rightarrow e^+e^-+$ jets production using 6.2 fb^{-1} of data collected with the CDF detector in run II. The CDF detector is described in detail elsewhere [2]. This measurement follows previous studies on $Z/\gamma^* \rightarrow e^+e^-+$ jets at CDF [3]. The measured cross sections are corrected back to particle level and compared to next-to-leading order (NLO) pQCD predictions including non-perturbative contributions. Inclusive jet differential cross section as a function of p_T^{jet} [18] in events with at least one and two jets in the final state, and the total cross section as a function of inclusive jet multiplicity are measured [19].

II. MONTE CARLO SIMULATION

Monte Carlo simulated samples are used to model the $Z/\gamma^* \rightarrow e^+e^-+$ jets signal reconstruction, estimate background contributions, unfold the measurements back to the particle level, and evaluate non-pQCD corrections applied to the NLO predictions. ALPGEN v2.10' interfaced to PYTHIA v6.325 [4] is used as event generator, with CTEQ5L parton distribution function (PDF) for the colliding proton and antiproton [5]. Tune BW parameters are employed to govern the underlying event. A full CDF detector simulation based on GEANT3 [8] is applied to the generated samples and the GFLASH [9] package is used to simulate the energy deposition in the calorimeter.

III. EVENT SELECTION

Events are collected using a three-level trigger system [10]. At the first-level trigger, events are required to have a central electromagnetic calorimeter cluster ($|\eta| < 1$) with $\mathrm{E_T}$ above 8 GeV and an associated track with p_T above 8 GeV/c. Similarly, at the second-level (third-level) trigger a central electromagnetic cluster with $\mathrm{E_T} > 16$ GeV ($\mathrm{E_T} > 18$ GeV) and an associated track with $p_T > 8\ GeV/c$ ($p_T > 9\ GeV/c$) are required. Events with a reconstructed primary vertex with z position within 60 cm from the nominal interaction point are selected. Electrons are identified offline on the basis of tracking, calorimeter and shower information, following the criteria described in [11]. A $Z/\gamma^* \rightarrow e^+e^-$ boson is identified requiring two reconstructed electrons with $\mathrm{E_T} > 25\ GeV$, and with invariant mass in the range $66 \leqslant M_{ee} \leqslant 116\ GeV/c$. One electron has to be central ($|\eta^e| < 1$), while the second electron can be either central or forward with $1.2 < |\eta^e| < 2.8$. Electron identification efficiencies are evaluated on data with a tag-leg versus probe-leg method. $Z/\gamma^* \rightarrow e^+e^-$events are selected requiring one electron leg to pass a set of tight identification cuts (tag-leg), and the other electron leg to meet kinematic requirements (probe-leg). The second leg is then used as a probe electron to evaluate the efficiencies of trigger and identification requirements. The resulting efficiencies are used to evaluate the $Z/\gamma^* \rightarrow e^+e^-$ inclusive cross section, which is checked against the next-to-leading order prediction and the published CDF result [11].

IV. JET RECONSTRUCTION

Jets are reconstructed in data and Monte Carlo simulated events from the energy deposits in the calorimeter towers with transverse momenta [20] above 0.1 GeV/c. Jets are searched for using the midpoint algorithm [12] with cone radius $R = 0.7$ and a merging/splitting fraction of 0.75, starting from seed towers with transverse momenta above 1 GeV/c. The same algorithm is applied to the final state particles in the Monte Carlo generated events, excluding Z/γ^* decay products, to define jets at the particle level. The measured jet transverse momentum p_T^{jet} systematically underestimates that of the particle-level jet. For p_T^{jet} values about 30 GeV/c, the jet transverse momentum is underestimated by about 30%. The systematic shift decreases with increasing p_T^{jet} down to about 11% for $p_T^{jet} > 200$ GeV/c. This is mainly attributed to the presence of inactive material and the non-compensating nature of the calorimeter [13]. An average correction, as a function of p_T^{jet} and y^{jet}, is applied to the measured p_T^{jet} to account for these effects [14]. The measured p_T^{jet} also includes contributions from multiple p$\bar{\text{p}}$ interactions per crossing at high instantaneous luminosity. Multiple interactions are identified via the presence of additional primary vertices reconstructed from charged particles. For each jet, p_T^{jet} is corrected for this effect by removing a certain amount of transverse momentum, $\delta^{\mathrm{mi}}_{\mathrm{p_T}} = 1.06 \pm 0.32$ GeV/c, for each additional primary vertex in the event, as determined from data [14]. After these corrections, jets with $p_T^{jet} \geqslant 30\ GeV/c$ and $|y^{jet}| \leqslant 2.1$ are selected. A minimum distance between the jets and the electrons ($\Delta \mathrm{R_{e-jet}} > 0.7$) is also required. The measured jet cross sections are corrected for acceptance and smearing effects back to the particle level using ALPGEN+PYTHIA-TUNE BW Monte Carlo event samples, and a bin-by-bin unfolding procedure that also accounts for the efficiency of the $Z/\gamma^* \rightarrow e^+e^-$ selection criteria.

V. BACKGROUNDS ESTIMATION

Background estimation is done both with Monte Carlo and data-driven techniques. The main background contribution arises from inclusive-jets and W+jets events, and is estimated from data. An inclusive jet data sample is employed to evaluate the probability f_e^{jet} of a jet to be mis-identified as an electron, parametrized as a function of p_T^{jet}. Then W + jets events with exactly one reconstructed central electron are selected in the same data sample used for the measurement, and each electron-jet pair which fulfills the Z/γ^* kinematic requirements of the measurement is considered as a $Z/\gamma^* \rightarrow e^+e^-$ candidate. The background estimation is finally obtained assigning to each electron-jet candidate the probability f_e^{jet} associated to the jet. Other contributions, coming from electroweak processes and $t\bar{t}$ events, are computed using MC sample. Figure 1 shows the invariant mass distribution of reconstructed $Z/\gamma^* \rightarrow e^+e^-$ in data compared to background plus Monte Carlo signal prediction, in events with $\geqslant 1$ jet and $\geqslant 2$ jets in the final state. The number of estimated background events and data event yields for $\geqslant 1$, 2, 3 and 4 jets are reported in table I.

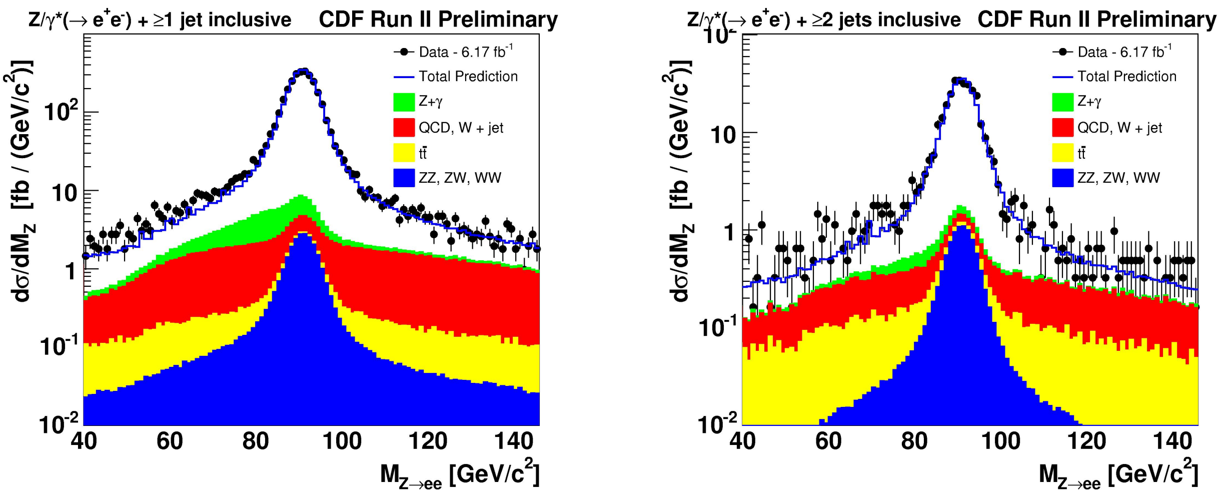

FIG. 1: Data and signal plus background estimation within Z mass window and on side bands, in (left) $Z+ \geqslant 1$ jet and (right) $Z+ \geqslant 2$ jets events.

CDF Run II Preliminary

Backgrounds	**Estimated events in 6.17 fb^{-1}**			
	Z + $\geq$ 1 jet	**Z + $\geq$ 2 jets**	**Z + $\geq$ 3 jets**	**Z + $\geq$ 4 jets**
QCD, W+Jet	502.1 ± 75.3	67.5 ± 10.1	7.6 ± 1.1	0.7 ± 0.1
$Z/\gamma^* \rightarrow e^+e^- + \gamma$	483.8 ± 145.1	32.0 ± 9.6	1.8 ± 0.5	0.1 ± 0.0
WW, ZZ, ZW	164.0 ± 49.2	61.5 ± 18.5	6.3 ± 1.9	0.5 ± 0.2
$t\bar{t}$	49.5 ± 14.9	29.8 ± 9.0	4.6 ± 1.4	0.6 ± 0.2
$Z/\gamma^* \rightarrow \tau^+\tau^-$ + jet	16.3 ± 4.9	0.0 ± 0.0	0.0 ± 0.0	0.0 ± 0.0
Total Backgrounds	1216 ± 172	191 ± 25	20.3 ± 2.7	1.8 ± 0.3
Data	20032 ± 142	2130 ± 46	187 ± 13.7	15.0 ± 3.9

TABLE I: Estimated background events in 6.17 fb^{-1} for $Z/\gamma^* \rightarrow e^+e^- + \geq 1$, 2, 3 and 4 jets compared to data yield.

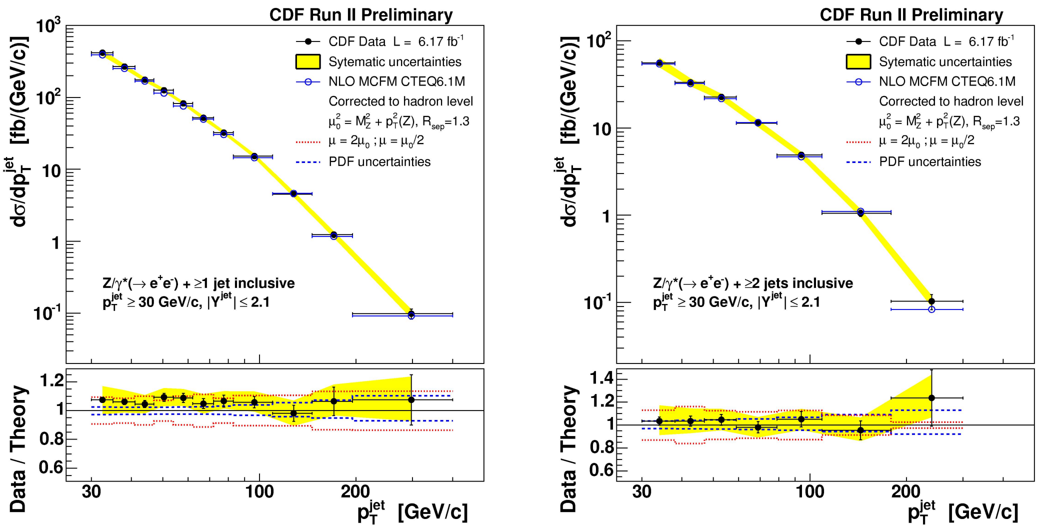

FIG. 2: Measured inclusive jet differential cross section as a function of p_T^{jet} (black dots) in $Z/\gamma^* + \geqslant 1$ jet and $Z/\gamma^* + \geqslant 2$ jets events compared to NLO pQCD predictions (open circles). The shaded bands show the total systematic uncertainty, except for the 5.8% luminosity uncertainty. The dashed and dotted lines indicate the PDF uncertainty and the variation with μ_0 of the NLO pQCD predictions, respectively.

VI. SYSTEMATIC UNCERTAINTIES

Several sources of systematic uncertainty to the measured cross section have been considered. The uncertainties on trigger and electron ID efficiencies are evaluated assuming a binomial distribution and the propagated uncertainty on the cross sections is 0.2%. The jet energies are varied by 2% at low p_T^{jet} and up to 2.7% at high p_T^{jet} to account for the uncertainties on the absolute energy scale in the calorimeter [14]; this introduces uncertainties on the final measurements which vary between 5% at low p_T^{jet} and 15% at high p_T^{jet}. The y^{jet} dependence of the average correction applied to p_T^{jet} introduces a 2% uncertainty on the measured cross sections, approximately independent of p_T^{jet}. The uncertainty on $\delta_{\mathrm{p_T}}^{\mathrm{mi}}$ translates into uncertainties between 1% and 10% on the measured cross sections. A conservative 15% uncertainty is assigned to the QCD, W+jets and decay-in-flight background contribution, which translates into a 0.5% uncertainty in the final results. A 30% uncertainty is assigned to the rest of the background contributions, which are evaluated with Monte Carlo simulation, leading to uncertainties between 1% and 3% on the measured cross sections. Positive and negative deviations with respect to the measured cross section values are added separately in quadrature to define the total systematic uncertainty. Finally the measurement is affected by an overall 5.8% uncertainty on the quoted total integrated luminosity.

VII. NEXT-TO-LEADING ORDER PREDICTION

The NLO predictions are computed using the MCFM program [15]. The CTEQ6.1M PDFs[16] are employed and the renormalization and factorization scales are set to $\mu_0^2 = \mathrm{M_Z^2} + \mathrm{p_T^2(Z)}$. Variation of the renormalization and factorization scales by a factor of two and half induces a change between 10% and 15% in the theoretical predictions. The uncertainty on the PDF is calculated with the Hessian method [17] and the corresponding uncertainties on the predictions vary from 2% at low p_T^{jet} to 15% at high p_T^{jet}.
The theoretical predictions include parton-to-particle level correction factors that account for underlying event and fragmentation processes. These non-perturbative effects are estimated with PYTHIA-TUNE A Monte Carlo simulation. The correction is obtained evaluating the ratio of the p_T^{jet} and N_{jet} distributions between particle-level jets and parton-level jets reconstructed turning off both the interaction between proton and antiproton remnants and the string fragmentation in the Monte Carlo samples.

VIII. RESULTS

Figure 2 shows the measured inclusive differential cross section in $Z/\gamma^* + \geqslant 1$ jet and $Z/\gamma^* + \geqslant 2$ jets events, for jets with $p_T^{jet} \geqslant 30\ GeV/c$ and $|y^{jet}| \leqslant 2.1$. The measurements are well described by the NLO pQCD predictions. Figure 3 presents the measured cross section as a function of inclusive $Z/\gamma^* + \geqslant N_{jet}$ multiplicity up to $N_{jet} = 4$, compared with the available LO and NLO MCFM predictions. Data are followed by the NLO predictions, in the three-jets bin data suggest a similar LO-to-NLO k-factor than the one obtained for $Z/\gamma^* + \geqslant 1$ jet and $Z/\gamma^* + \geqslant 2$ jets results.

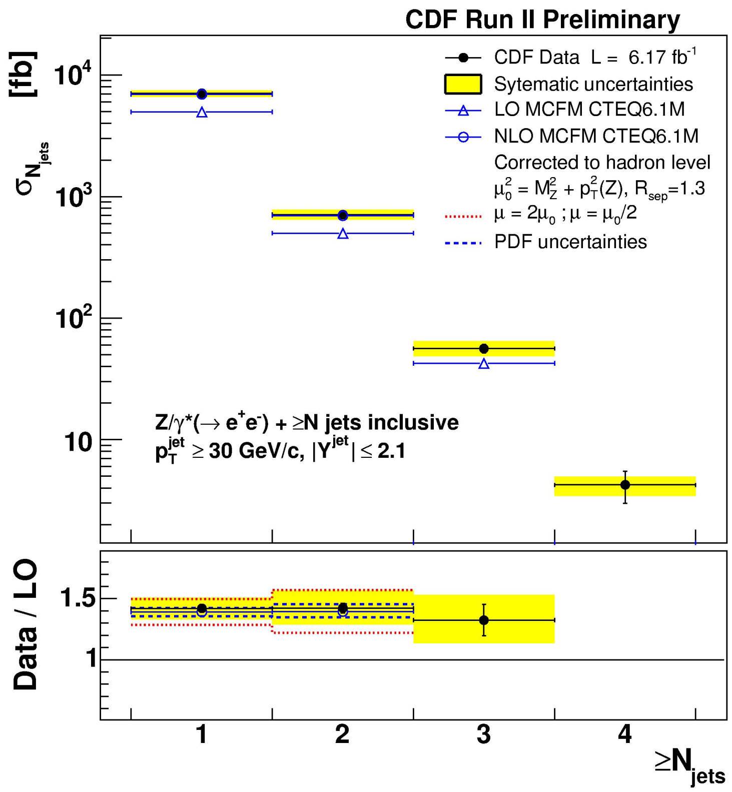

FIG. 3: (top) Measured total cross section for inclusive jet production in $Z/\gamma^* \to e^+e^-$ events as a function of N_{jet} compared to LO and NLO pQCD predictions. The shaded bands show the total systematic uncertainty, except for the 5.8% luminosity uncertainty. (bottom) Ratio of data and NLO to LO pQCD predictions as a function of N_{jet}. The dashed and dotted lines indicate the PDF uncertainty and the variation with μ_0 of the NLO pQCD predictions, respectively.

Acknowledgments

We thank the Fermilab staff and the technical staffs of the participating institutions for their vital contributions. This work was supported by the U.S. Department of Energy and National Science Foundation; the Italian Istituto Nazionale di Fisica Nucleare; the Ministry of Education, Culture, Sports, Science and Technology of Japan; the Natural Sciences and Engineering Research Council of Canada; the National Science Council of the Republic of China; the Swiss National Science Foundation; the A.P. Sloan Foundation; the Bundesministerium für Bildung und Forschung, Germany; the Korean World Class University Program, the National Research Foundation of Korea; the Science and Technology Facilities Council and the Royal Society, UK; the Institut National de Physique Nucleaire et Physique des Particules/CNRS; the Russian Foundation for Basic Research; the Ministerio de Ciencia e Innovación, and Programa Consolider-Ingenio 2010, Spain; the Slovak R&D Agency; and the Academy of Finland.

[1] D.J. Gross and F. Wilczek, Phys. Rev. D 836331973
[2] F. A be, et al., Nucl. Instrum. Methods Phys. Res. A **271**, 387 (1988); D. Amidei, et al., Nucl. Instum. Methods Phys. Res. A **350**, 73 (1994); F. Abe, et al., Phys. Rev. D **52**, 4784 (1995); P. Azzi, et al., Nucl. Instrum. Methods Phys. Res. A **360**, 137 (1995); The CDFII Detector Technical Design Report, Fermilab-Pub-96/390-E
[3] The CDF Collaboration Phys. Rev. Lett. **100** 102001 (2008).
[4] T. Sjostrand et al., High-Energy-Physics Event Generation with PYTHIA 6.1, Comput. Phys. Commun. **135**, 238 (2001).
[5] H.L. Lai *et al.*, Eur. Phys. J. C **12**, 375 (2000).
[6] T. Affolder *et al.* (CDF Collaboration), Phys. Rev. D **65**, 092002 (2002)
[7] O. Saltó, Ph.D. Thesis, U.A.B., Barcelona (2008).
[8] R. Brun *et al.* Tech. Rep. CERN-DD/EE/84-1, 1987.
[9] G. Grindhammer, M. Rudowicz, and S. Peters, Nucl. Instrum. Methods A **290**, 469 (1990).
[10] B. L. Winer, Int. J. Mod. Phys. A **16S1C**, 1169 (2001).
[11] D. Acosta *et al.* (CDF Collaboration), Phys. Rev. Lett. **94**, 091803 (2005).
[12] A. Abulencia *et al.* (CDF Collaboration), Phys. Rev. D **74**, 071103(R) (2006).
[13] S.R. Hahn *et al.*, Nucl. Instrum. Methods A **267**, 351 (1988).
[14] A. Bhatti *et al*, Nucl. Instrum. Methods A **566**, 375 (2006).
[15] J. Campbell and R.K. Ellis, Phys. Rev. D **65** 113007 (2002).
[16] J. Pumplin, *et al.*, JHEP **0207** 012 (2002).
[17] J. Pumplin, *et al.*, Phys. Rev. D **65** 014013 (2001).
[18] Coordinates are referred to a cylindrical system with the z axis along the beam line, polar angle θ and azimuthal angle ϕ. Transverse energy and momentum are defined as $E_T = E\ \sin\theta$ and $p_T = p\ \sin\theta$, pseudorapidity and rapidity as $\eta = -\ln(\tan(\frac{\theta}{2}))$ and $y = \frac{1}{2}\ln(\frac{\mathrm{E+p_z}}{\mathrm{E-p_z}})$.
[19] Results, including also cross sections as a function of y^{jet}, are reported in http://www-cdf.fnal.gov/physics/new/qcd/zeejets_10
[20] The momentum is computed using the energy and the position with respect to the primary interaction vertex.